

Local magnetism in granular iron/iron oxide nanostructures by phase- and site-selective x-ray magnetic circular dichroism

Luca Signorini, Luca Pasquini, Federico Boscherini, and Ennio Bonetti

Department of Physics and CNISM, University of Bologna, Viale C. Berti Pichat 6/2, I-40127, Bologna, Italy

Isabelle Letard

European Synchrotron Radiation Facility 6 rue Jules Horowitz, BP 220, F-38043, Grenoble Cedex, France

Sandrine Brice-Profeta

ENSEEG/LTPCM Domaine Universitaire, 1130 rue de la piscine, BP 75, F-38402, Saint-Martin d'Hères Cedex, France

Philippe Saintavrit

IMPMC, UMR 7590, CNRS & UPMC 4 place Jussieu, F-75252 Paris cedex 05, France

(Received 6 February 2006; published 21 July 2006)

We present a study of the local magnetic properties of iron/iron oxide granular nanostructures by x-ray magnetic circular dichroism (XMCD). Metallic iron (α -Fe) nanoparticles, with average sizes ranging from 5 to 13 nm, are embedded in a nanocrystalline oxide matrix composed of both magnetite (Fe_3O_4) and maghemite ($\gamma\text{-Fe}_2\text{O}_3$). These granular samples were synthesized by cold compacting core-shell nanoparticles, in which a 2–3 nm-thick oxide layer surrounds the iron particles, synthesized by inert gas condensation. By exploiting the chemical selectivity and site sensitivity of XMCD, we were able to separate the magnetic contributions of the metallic core and of the two oxide phases present in the matrix and to study their behavior as a function of iron particle size and applied magnetic induction field. We detected the presence of a significant spin canting, predominantly affecting the octahedral sites of Fe in the oxide phase, and studied its dependence on the degree of structural disorder and applied magnetic induction field.

DOI: [10.1103/PhysRevB.74.014426](https://doi.org/10.1103/PhysRevB.74.014426)

PACS number(s): 75.75.+a, 61.10.Ht, 61.46.-w, 81.07.Bc

I. INTRODUCTION

The structure and properties of ultra-fine particles and granular nanostructures attract both fundamental and technological research interest, motivated by the challenge of discovering and understanding phenomena related to size and surface effects.¹ A number of synthesis routes are being currently employed and continuously improved; the aim is to improve the control over the size distribution, surface morphology, and stability of nanostructures.² Magnetic core-shell nanoparticles, constituted by a ferromagnetic core surrounded by a weakly magnetic or antiferromagnetic oxide shell, have potential applications in magnetic recording technology^{3,4} and they can be easily compacted in order to produce metal/oxide granular samples in which metal nanoparticles are uniformly embedded in an oxide matrix. For instance, Fe/Pt or Co/CoO core-shell nanoparticles are nowadays studied as candidates to provide media with very high magnetic recording densities,⁵ while oxide based nanostructures have many useful application in spintronics.⁶

A suitable way to synthesize granular nanostructures is a two step process in which the Inert Gas Condensation (IGC) method⁷ is used to produce metallic nanoparticles and the oxide shell is the result of a controlled surface oxidation process. The oxide shell, besides protecting against further oxidation, represents the effective medium for transmission of exchange interactions and conduction electrons between the ferromagnetic metallic cores.

The iron/iron oxide core-shell system is certainly one of the most studied materials in this class.^{8–10} It is generally

accepted that, for particle sizes above 2 nm, the magnetic moment per atom and the lattice parameter of the α -Fe cores are equal to those of bulk α -Fe, while the oxide shell consists of a mixture of heavily strained magnetite (Fe_3O_4) and maghemite ($\gamma\text{-Fe}_2\text{O}_3$), i.e., the two iron oxides with a spinel structure.^{11,12} The oxide layer is only 2–3 nm thick and is composed of very fine crystallites, the size of which is similar. In nanostructured magnetically ordered materials, the high density of interfaces, defects, and, more generally, the presence of structural disorder, gives rise to the misalignment of atomic magnetic moments.^{10,13} For the sake of simplicity, we will generally designate all these magnetic disorder phenomena as spin *canting*, irrespective of its origin being a surface-, a size- or a disorder-driven effect(s).

X-ray Magnetic Circular Dichroism (XMCD) originates from a coupling between the photon spin and the atomic magnetic moment; upon application of an external magnetic induction field, this gives rise to a difference between the absorption cross sections measured with the magnetic field parallel or antiparallel to the photon wave vector. XMCD was first observed in 1987 by Schütz *et al.*¹⁴ at the Fe K edge. In the soft x-ray range, it was first measured at the Ni $L_{2,3}$ edges three years later by Chen *et al.*¹⁵ In addition to the chemical selectivity of x-ray absorption spectroscopy (XAS), XMCD gives information on the spin and orbital magnetic moments of the excited atom. Moreover, the intensity of the XMCD signal measured for a given atom in a given site is proportional to the projection of the magnetic moment of the absorbing atom on the direction of the applied magnetic field.¹⁶ This also allows to record hysteresis loops

corresponding to a given element for a sample containing several different magnetic elements.

In this paper, we employ XMCD at the $\text{Fe}L_{2,3}$ edges to study the magnetic behavior of granular iron/iron oxide nanostructures obtained by compacting Fe/Fe oxide nanoparticles prepared by IGC and post-oxidation. The presence of three different magnetic phases, i.e., metallic iron, magnetite, and maghemite, and the quite complex nanocrystalline structure of this kind of sample, exhibiting both size-dependent^{11,17,18} and disorder-driven effects,¹⁹ make this study particularly challenging, both from a fundamental physics and experimental point of view. In particular, we used XMCD to separate and quantify different magnetic contributions due to the three phases and we independently studied their behavior as a function of the applied magnetic induction field and metallic particle dimensions. We also investigated in more detail the magnetic behavior of the disordered oxide matrix. In this way, we were able to compare the magnetic behavior of nanometric maghemite and magnetite grains to that of their coarse grained counterparts and, more importantly, we found evidence for a disorder-driven enhancement of spin canting for iron atoms in octahedral sites. Since XMCD has mostly been applied to the study of two dimensionally ordered systems or ordered bulk materials, in the present study we illustrate a significant extension of the field of application of the technique to the study of highly disordered nanocrystalline solids.

II. EXPERIMENTAL

Iron nanoparticles were synthesized using the IGC technique: 99.98% pure iron was evaporated from a tungsten crucible 133 Pa of 99.9999% pure He. Nanoparticles are formed by homogeneous nucleation of metallic vapors and by convection they collect on a rotating drum cooled by liquid nitrogen. After restoring high-vacuum conditions (10^{-5} Pa), the passivation procedure was initiated by slowly admitting pure O_2 into the growth chamber. A pressure of 133 Pa was attained in about one hour. Finally, the nanoparticles were exposed to 1.2 kPa of He for 24 h. The oxidation procedure deposits an iron oxide (Fe_xO_y) layer on the metallic cores, resulting in the core-shell morphology.¹¹ Oxidized particles ($\text{Fe}/\text{Fe}_x\text{O}_y$) were then scraped from the collection surface and cold-compacted in the form of pellets in a high vacuum under a uniaxial pressure of 1.5 GPa, in order to obtain granular nanostructures. The mean size of the nanoparticles was controlled by varying the evaporation rate by adjusting the evaporator heating current. In this way, three samples were prepared: FeO5, FeO9, and FeO13, where the final number represents D , the average core diameter in nm, determined as described later. Some of the present authors¹¹ have previously reported an XAS investigation at the Fe and O K edges on similar samples; it was found that the volume fraction of maghemite decreases from 94% to 17% with an increasing core diameter in the range 7–21 nm. The high degree of structural disorder for smaller particles was suggested to cause an enhanced rate of transformation from magnetite to maghemite in the oxygen rich atmosphere during growth.

X-ray Diffraction (XRD) was carried out using a Rigaku DMAX IIIC diffractometer with $\text{Cu-K}\alpha$ radiation ($\lambda = 1.54056 \text{ \AA}$) and a graphite monochromator in the diffracted beam. The diffraction profiles were analyzed using the MAUD software package,²⁰ which performs a Rietveld full profile fitting.²¹

Fe $L_{3,2}$ edge XMCD measurements were performed at the BACH beamline of the ELETTRA Synchrotron Radiation Laboratory (Trieste, Italy), operated at 2.4 GeV. A pair of APPLE-II undulators²² provided the photon source and a spherical grating monochromator with a groove density of 400 lines/mm was used. The first harmonic of the undulator radiation was used and the flux on the sample was approximately 7×10^{11} photons/s. The circular polarization rate of the x-ray beam was close to 100% and the resolving power of the monochromator was ~ 1500 . XMCD spectra were collected with a step of 0.2 eV.

Samples were placed in a ^4He cryostat developed by Kappler and Saintavit.²³ With this apparatus the sample temperature can be set between 300 and 1.5 K, while the external magnetic induction field is generated by a superconducting coil and can be reversed from -7 to 7 T in less than 15 minutes. The direction of the applied field was parallel or antiparallel to the wave vector of the impinging x-ray beam; all spectra were collected with the sample surface perpendicular to the beam itself. The samples were directly glued on the sample holder with conductive silver paint, in order to ensure good electrical and thermal conductivity. XAS spectra were collected in the Total Electron Yield (TEY) mode by recording the sample drain current as a function of photon energy.

Two series of measurements were performed at the temperature of 100 K for different values of the applied magnetic induction field B : all samples were investigated at $B = 5$ T, while only samples FeO5 and FeO13, the least and the most concentrated in $\alpha\text{-Fe}$ content, were also measured at $B = 2$ T. Measurements were performed by reversing both the direction of the applied magnetic induction field and the photon helicity in order to minimize systematic errors that could adversely affect the spectra, as explained later.

XMCD is defined as the difference between the x-ray absorption cross section for right-handed and left-handed photons in the presence of an applied magnetic field parallel to the photon wave vector.^{24,25} Thus, the dichroic signal is $\sigma_{\text{XMCD}} = \sigma^{\uparrow\uparrow} - \sigma^{\uparrow\downarrow}$, where σ^{ab} denotes the cross section with a representing the helicity of the photon and b the direction of the applied magnetic field. $a = \uparrow(\downarrow)$ when the photon is left (right) handed, while $b = \uparrow(\downarrow)$ when the magnetic field is parallel (antiparallel) to the photon wave vector. It is well known²⁶ that, in the electric dipole approximation, reversing the magnetic field direction is equivalent to changing the incoming photon helicity: $\sigma^{\uparrow\downarrow} = \sigma^{\downarrow\uparrow}$ and $\sigma^{\uparrow\uparrow} = \sigma^{\downarrow\downarrow}$. From this point of view, the same dichroic signal should, in principle, be obtained, reversing either the beam helicity or the applied field; as matter of fact, the two procedures often provide slightly different results because of experimental setup limitations or various systematic errors (e.g., the sensitivity of the TEY detection mode to the orientation of the magnetic field and slight changes in the beam position on the sample when changing the photon helicity). In order to minimize

TABLE I. Results of Rietveld analysis of XRD spectra.

	Crystallite size (nm)	Microstrain (10^{-3})	Volume fraction
FeO5			
α -Fe	5.3 ± 0.6	11 ± 2	11%
Fe_xO_y	2.5 ± 0.6	12 ± 3	89%
FeO9			
α -Fe	9.3 ± 0.4	6.1 ± 0.7	30%
Fe_xO_y	2.0 ± 0.3	9 ± 2	70%
FeO13			
α -Fe	13.1 ± 0.4	4.0 ± 0.3	48%
Fe_xO_y	2.4 ± 0.1	7 ± 2	52%

these systematic errors, the XMCD spectra reported in this paper were all obtained by averaging tens of equivalent spectra collected by alternatively reversing beam helicity and orientation of the magnetic induction field. Reported XMCD spectra are given by $\sigma_{\text{XMCD}} = [(\sigma^{\uparrow\downarrow} + \sigma^{\downarrow\uparrow}) - (\sigma^{\uparrow\uparrow} + \sigma^{\downarrow\downarrow})]/2$ while isotropic absorption spectra were calculated as $\sigma_{\text{ISO}} = (\sigma^{\uparrow\downarrow} + \sigma^{\downarrow\uparrow} + \sigma^{\uparrow\uparrow} + \sigma^{\downarrow\downarrow})/4$. The latter spectra were found to be identical to the XAS spectra measured without applied magnetic induction and sample magnetization. No corrections for the sample geometry or the partial beam polarization are necessary in our experimental conditions.

Spectra of bulk α -Fe, magnetite, and maghemite, were collected as references on the BACH beamline and also at the SU23 beamline on the Super-ACO storage ring of the (former) LURE laboratory (Orsay, France); measurements on these reference samples were performed at $T=5$ K and $B=2$ T.

III. DATA ANALYSIS

A. Structural characterization

XRD profiles of the three nanosamples, as previously reported,^{10–12} show the presence of two different phases: metallic α -Fe, and an oxide with a spinel structure that can be identified either as Fe_3O_4 or γ - Fe_2O_3 . The presence of hematite, α - Fe_2O_3 , can be safely excluded. The Rietveld analysis (the results of which are reported in Table I) allowed us to determine crystallite size, root squared microstrain ($\langle \varepsilon^2 \rangle^{1/2}$), and concentrations of these two phases. An observed severe peak broadening (not shown here) indicates that the oxide matrix is composed by ultrafine crystallites with dimensions in the range 2–3 nm.

The increase of the microstrain in the α -Fe cores with decreasing diameter reflects the enhanced relative number of Fe atoms located at the metal/oxide interface and most likely subjected to local stresses; also, the microstrain of the oxide matrix increases with decreasing dimension of the cores. This behavior can be attributed to the greater volume concentration of grain boundaries and low coincidence interfaces of the shells grown around smaller metallic particles.^{11,27}

B. XMCD measurements

In order to provide a consistent normalization, raw XAS spectra were divided by the value of the x-ray absorption at the maximum of the L_3 edge of the isotropic spectra. As an example, the XAS spectra for sample FeO9 measured with both beam helicities and obtained using this procedure are reported in Fig. 1(b). The XMCD signals (multiplied ten times) for the three investigated samples are also shown in Fig. 1 (open circles), while similarly normalized reference spectra of α -Fe, magnetite, and maghemite are reported in

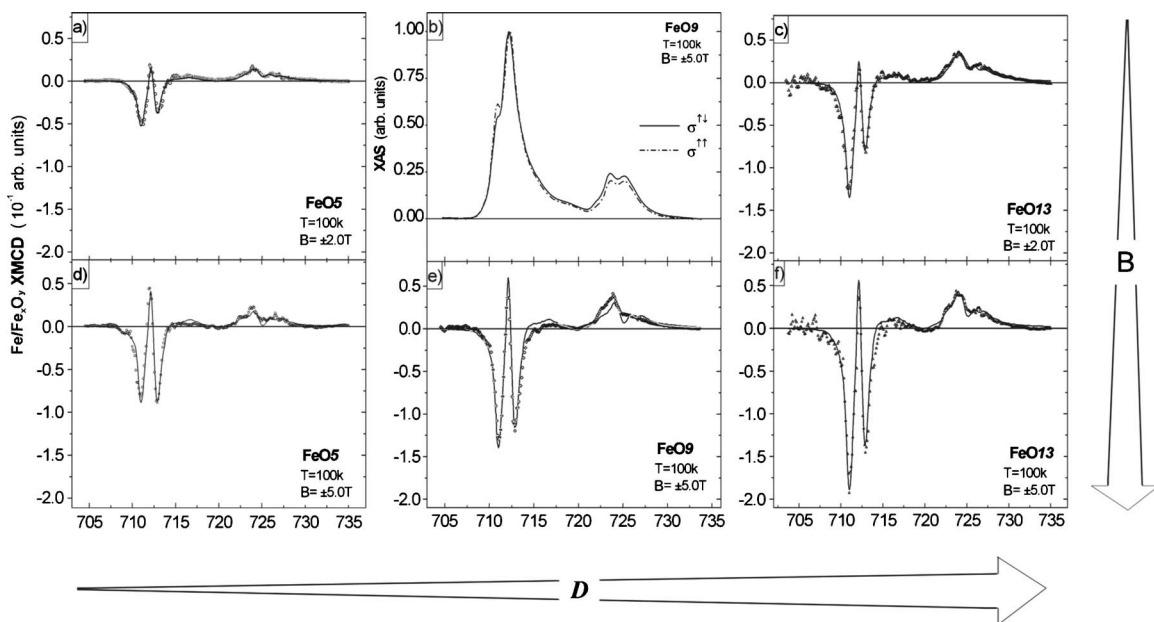


FIG. 1. XAS and XMCD spectra at the Fe- $L_{3,2}$ edges. Continuous lines report the best fit of experimental points (open circles). The XAS spectrum of sample FeO9 is shown in (b) for both relative orientations of the applied magnetic induction field and photon beam helicity. XMCD spectra measured with $B=2$ T are shown in (a) and (c) while XMCD spectra measured at $B=5$ T are reported in (d), (e), and (f).

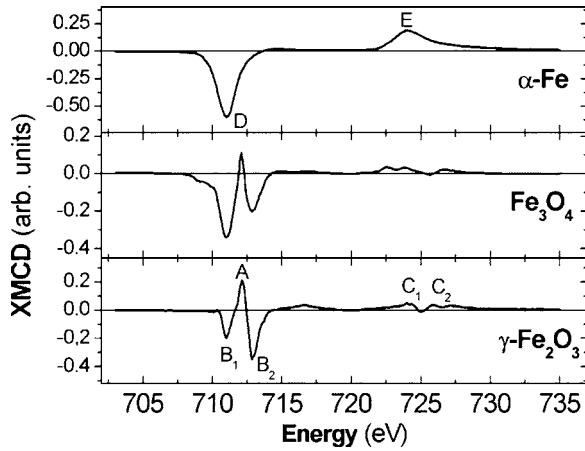


FIG. 2. Reference XMCD spectra.

Fig. 2. From multiplet calculations, we know the exact normalizations for Fe^{2+} and Fe^{3+} isotropic and XMCD spectra. This yields the normalization for Fe_3O_4 and $\gamma\text{-Fe}_2\text{O}_3$, as plotted in Fig. 2. The normalization for $\alpha\text{-Fe}$ is not as straightforward because multiplet calculations are not so accurate for metals. The $3d$ shell of iron atoms in $\alpha\text{-Fe}$ is believed to host around 6.5 electrons,²⁸ as in the case of Fe^{2+} . The integral of the isotropic spectra for $\alpha\text{-Fe}$ and Fe^{2+} should be roughly the same. This sets the normalization of $\alpha\text{-Fe}$ spectra with those of $\gamma\text{-Fe}_2\text{O}_3$ and Fe_3O_4 .

It is evident that the XMCD spectra of the samples in Fig. 1 show the same main features as those reported in Fig. 2 for spinel oxides. The L_3 edge region consists, in fact, of three different peaks: from lower to higher energy, the first (B_1) and the third one (B_2) are negative, while the central peak (A) is positive. On the contrary, the L_2 region is characterized by two smaller positive peaks (C_1 and C_2). It is well known that the negative B_1 and B_2 peaks arise from Fe atoms occupying octahedral sites, the magnetic moments of which are parallel to the applied magnetic field.^{29–33} Atoms in tetrahedral sites are antiferromagnetically coupled to octahedral ones and, consequently, their magnetic contribution to XMCD is positive at the L_3 edge (peak A). Besides, while both magnetite and maghemite cubic unit cell hosts 8 Fe^{3+} ions with tetrahedral coordination, the different relative intensities of peaks B_1 and B_2 in XMCD spectra is due to the different occupation number of octahedral sites in the two oxides: in each cubic unit cell, magnetite hosts 8 Fe^{2+} and 8 Fe^{3+} cations randomly sharing the octahedral sites, while only 13.33 Fe^{3+} ions, on average, are present in maghemite.^{32,34–36} At the L_2 edge, the contributions from octahedral and tetrahedral ions reverse in sign and give rise to peaks C_1 and C_2 .^{31,32,37} The spectra reported for all samples and magnetic induction fields in Fig. 1 are qualitatively similar to those reported¹⁸ for isolated Fe-Fe oxide core-shell nanoparticles at $B=0.5$ T.

We now qualitatively discuss the XMCD spectra of the samples. We notice that with an increasing core dimension, the negative peaks at the L_3 edge and the positive peaks at the L_2 edge increase in intensity; moreover, the first negative peak at the L_3 edge increases in amplitude more than the second one. This can be explained by noting that the XMCD

TABLE II. Results of the fitting of XMCD spectra, obtained as described in the text.

Sample	Applied Field (T)	a_1 $\alpha\text{-Fe}$ (10^{-3})	a_2 Fe_3O_4 (10^{-3})	a_3 $\gamma\text{-Fe}_2\text{O}_3$ (10^{-3})
FeO5	2	45 ± 2	16 ± 5	107 ± 5
FeO5	5	22 ± 4	128 ± 7	194 ± 7
FeO9	5	53 ± 4	128 ± 8	217 ± 12
FeO13	2	129 ± 4	52 ± 4	207 ± 8
FeO13	5	122 ± 7	198 ± 18	299 ± 13

of $\alpha\text{-Fe}$ is characterized by a strong negative peak D (centered at the same position of peak B_1 and partially superposed to peak A exhibited by the oxides) and a smaller positive peak E approximately at the same position of the C_1 peak. The change of the intensity of the XMCD features with core dimensions is thus a consequence of the increase of the metal content in the sample; a further contribution can be due to the decrease of the microstrain of the whole system, in particular, of the oxide matrix. In fact, it has already been found that the magnetization of the oxide strongly decreases with an increasing value of the matrix microstrain.¹⁰

Comparing the overall amplitude of the sample and reference XMCD spectra, we note that the former are quite weaker than the latter. This is not surprising, since it is well known that nanocrystalline and strained materials generally exhibit a reduction of saturation magnetization and thus of the XMCD amplitude because of strong spin canting of the atoms situated on interfaces and grain boundary regions.³⁸ We note that the XMCD amplitude of the samples increases with the applied magnetic induction field, indicating that the magnetization is not saturated below 2 T and at 100 K. Since it is known that in spinel oxides the amplitude of the dichroic signal at the L_3 edge is roughly proportional to the macroscopic magnetization,³³ this behavior is expected for these structurally and magnetically disordered systems.¹⁰ Furthermore, the described trend is compatible with previous SQUID measurements of magnetization performed at the same value of the applied field.¹⁰

In order to estimate the separate magnetic contributions of $\alpha\text{-Fe}$, Fe_3O_4 , and $\gamma\text{-Fe}_2\text{O}_3$ to the XMCD spectra of the samples, we performed a fit of the data based on a linear combination of the three reported reference XMCD signals. Fitting curves were calculated as

$$\text{XMCD}_{\text{fit}}(E) = a_1 \times \text{XMCD}_{\alpha\text{-Fe}}(E) + a_2 \times \text{XMCD}_{\text{Fe}_3\text{O}_4}(E) + a_3 \times \text{XMCD}_{\gamma\text{-Fe}_2\text{O}_3}(E), \quad (1)$$

in which the a_i coefficients are fitting parameters that quantify the contributions of the i th phase to the overall signal; best fits, which are shown in Fig. 1 as continuous lines, were obtained using the least squares method. The values of the a_i coefficients, that are linked to the absolute magnetic contributions of different phases to sample magnetization, are reported in Table II. The quality of the procedure is illustrated by the good agreement between the fitting curves and the

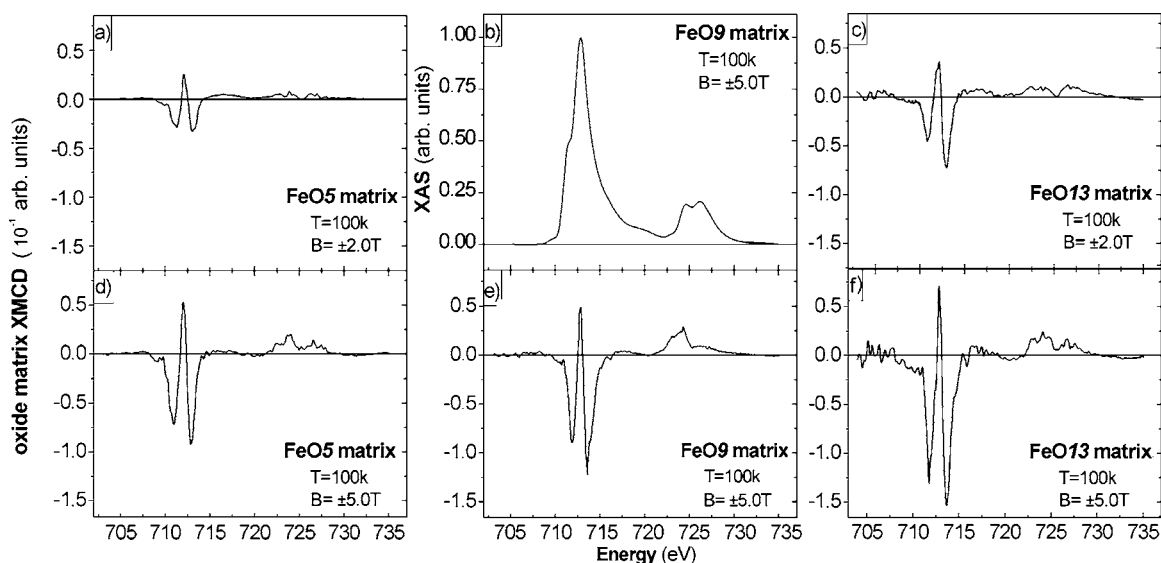


FIG. 3. Oxide matrix contribution to XMCD spectra. (a) and (c) measurements at $B=2$ T; (d), (e), and (f): measurements at $B=5$ T. The isotropic XAS spectrum of sample FeO9 is reported in (b).

experimental data. However, some words of caution are necessary. When recording XMCD spectra in the TEY mode in the soft x-ray range spectral distortions due to self-absorption are possible since the x-ray probe depth, although always longer, may become comparable to the electron probe depth, especially near the strong absorption edges. Various authors^{39,40} have quantitatively studied the problem. Quantitative studies⁴⁰ have found that spectral distortions are weaker in the normal incidence geometry, which is the one chosen by us in the present investigation. However, some distortions due to self-absorption may be present, especially since peaks due to the oxides and to the metal are partially superposed; a correction for self-absorption distortions appears quite complicated in the present case, due to the complex morphology of the samples, and was not attempted. Finally, it should be noted that for the weaker signals some systematic errors may be introduced by the procedure used in data treatment and normalization; these errors are probably larger than the statistical uncertainty of the fit. In conclusion, while we believe that the decomposition of the XMCD spectra bear a close relation to the contribution of each phase to the magnetic response, we avoid assigning a precise quantitative meaning to the fitting coefficients.

IV. DISCUSSION

In this paragraph we first discuss the magnetic behavior of the metal and oxide phases as a function of increasing core size and applied field and then we analyze in detail the oxide matrix, focusing on the contributions of Fe_3O_4 and $\gamma\text{-Fe}_2\text{O}_3$ and on the different magnetic features of iron atoms belonging to tetrahedral and octahedral sublattices.

A. Iron and oxide contributions to magnetization

As already pointed out, at a constant applied magnetic induction field, the contribution of $\alpha\text{-Fe}$ to the magnetization

increases with increasing core dimension (see the values reported in Table II). This behavior is compatible with previous magnetic measurements^{9,10} and can be understood as due to both the enhanced metal content and the decreased structural disorder.

Comparing now the XMCD spectra of samples FeO5 and FeO13, which were taken at two values of the applied field (2 T and 5 T), we see that the contribution of the oxide phases increases with the applied field. This shows that in granular nanostructures the oxide phases achieve magnetic saturation at considerably higher applied fields than in the corresponding coarse grained materials (in which a few hundreds mT are sufficient). This magnetic behavior can be attributed to the large fraction of Fe atoms set in interface regions and to the extremely high structural disorder of the matrix. In fact, at temperatures below 125 K, a progressive freezing of the magnetic moments of oxide grains, in agreement with the known local random distribution of the anisotropy energy barrier,¹⁰ is known to occur; we note that the $\text{Fe}/\text{Fe}_x\text{O}_y$ system exhibits a full spin-glass-like behavior at temperatures below about 20 K.¹⁰

In sample FeO13 the value of the a_1 coefficient relative to the Fe core does not change, within the error bars, upon raising the applied field from 2 to 5 T: the magnetization of the iron core is saturated at 2 T; this is compatible with previous results.¹⁰ The decrease of the a_1 coefficient in sample FeO5 is unexpected; a possible (maybe partial) explanation for this may lie in the quoted self-absorption spectral distortions.

B. Magnetic properties of the oxide matrix

In order to study the magnetic properties of the oxide matrix, we have subtracted the previously estimated contribution due to metallic cores from the XMCD signals and raw isotropic XAS spectra. In Fig. 3 we report the result of this procedure: the oxide matrix contribution to the XMCD spec-

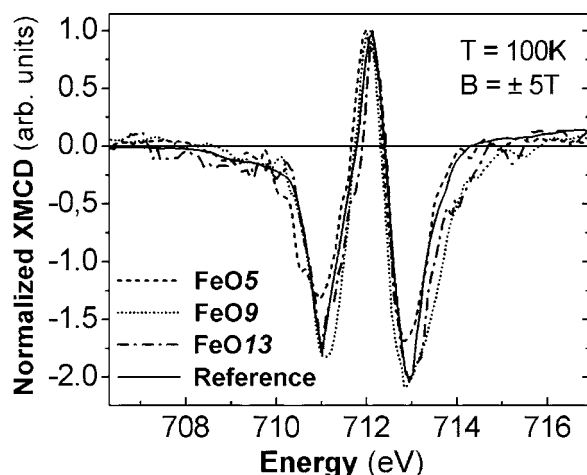


FIG. 4. Oxide matrix contribution to L_3 edge XMCD spectra measured at $B=5$ T. For comparison, also shown is a reference signal (40% Fe_3O_4 and 60% $\gamma\text{-Fe}_2\text{O}_3$).

tra of all the samples and the oxide matrix contribution to the isotropic XAS spectrum of sample FeO9 are shown.

An inspection of Fig. 3 shows that the XMCD amplitude slightly increases with increasing core dimensions, tending toward the greater amplitude exhibited by the reference samples. This trend is most probably caused by the decrease of structural, and consequently magnetic, disorder of the oxide that surrounds larger metal particles.^{10,11} Spin canting of the oxide phase has also been observed in isolated Fe-Fe oxide core shell nanoparticles.¹⁸ From Table II, we also notice that it is above all magnetite that increases its magnetic contribution to XMCD with an increasing applied field; in fact, the value of the a_2 fitting coefficient increases at least by a factor 4, while a_3 hardly doubles its value at $B=5$ T. This behavior may be simply attributed to a higher coercivity for Fe_3O_4 grains. However, a more complex phenomenon might be at the origin of this effect. During the fast and abrupt passivation process, ultrafine magnetite grains grow directly on the core surface in a disordered way, because of the extremely high oxidation speed and the lattice mismatch between oxide and metal. On the contrary, maghemite originates in a second step, growing on the external surface of the particle shell, through a further slower oxidation of magnetite. The growth process of $\gamma\text{-Fe}_2\text{O}_3$ is mediated by Fe^{2+} cations and vacancy diffusion^{41,11} that can give rise to structural reorganization and a lower degree of structural disorder. This mechanism could thus result in a smaller spin canting of maghemite compared to magnetite. Whatever the mechanism at the base of the higher field necessary to magnetize the magnetite component, the present result nicely illustrates the power of XMCD in discriminating the magnetic properties of different phases in the same sample.

C. Comparison of the magnetic properties of octahedral and tetrahedral sites in the oxide matrix

In order to compare the dichroic signal originating from the octahedral and tetrahedral sites in the oxide matrix we report in Fig. 4 the L_3 edge XMCD spectra obtained with a

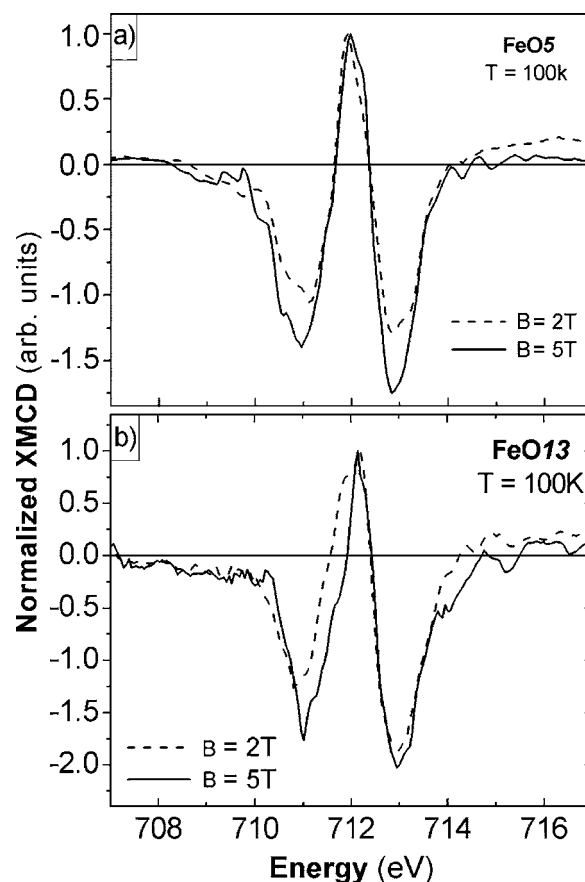


FIG. 5. A comparison between L_3 edge XMCD spectra measured at $B=5$ and 2 T: (a) sample FeO5 and (b) sample FeO13.

5 T applied field, normalized to equal height (and almost the same area) for peak A; we recall that peak A is due to the Fe ions occupying the tetrahedral sites. In doing so, we followed the approach developed by Brice-Profeta *et al.*^{32,33} In Fig. 4 we also report a reference spectrum obtained as a weighted linear combination of reference maghemite and magnetite spectra normalized in the aforesaid manner. The chosen weights, derived from Table II, are the average magnetic contributions of the two oxides to the matrix XMCD at $B=5$ T, i.e., respectively, 61% and 39%. In Fig. 5 we report similarly normalized spectra for samples FeO5 and FeO13 obtained for applied fields of 2 and 5 T.

It is clear from Fig. 4 that the spectra of samples FeO9 and FeO13 can be superposed quite well on the reference spectrum, and differences between negative peak intensities are within experimental uncertainty. On the contrary, sample FeO5 has less intense B_1 and B_2 peaks. This suggests that the higher structural disorder of sample FeO5 influences, in particular, spin canting of the octahedral sites. An inspection of Fig. 5 shows that both the samples FeO5 and FeO13 exhibit a reduced amplitude of peaks B_1 and B_2 (compared to peak A) at an applied magnetic induction field of 2 T. This implies that the magnetic contribution of Fe atoms belonging to octahedral sublattice is weakened, if compared to the tetrahedral one, when a less intense external field is applied, in particular, for the more highly disordered sample FeO5.

These results significantly extend the observation of overall spin canting for the oxide matrix reported for isolated

nanoparticles by Fauth *et al.*,¹⁸ since we are able to assign increased spin disorder preferentially to the octahedral sites. The same enhanced spin canting of Fe ions in the octahedral sublattice has been previously observed by XMCD in chemically synthesized maghemite nanoparticles of 2.7 nm average dimension³³ and has been suggested to be at the origin of the modifications of the Mössbauer spectrum of ball milled Fe/Fe₃O₄ nanocrystalline composite system.⁴² Despite the quite clear experimental evidence the origin of this selective spin canting awaits an explanation.

V. CONCLUSIONS

In conclusion, we have reported Fe L_{2,3} edge XMCD measurements of iron/iron oxide granular nanostructures obtained by cold compacting core-shell nanoparticles with core size in the range between 5–13 nm. Experimental XMCD spectra were fitted with a linear combination of reference dichroic signals of α -Fe, Fe₃O₄, and γ -Fe₂O₃ in order to discuss the separate magnetic contributions each phase to the overall magnetization.

As expected, the contribution of metallic iron to XMCD increases with increasing core dimension and, consequently, α -Fe content. The contribution of the disordered oxide matrix is found to increase when the applied field goes from 2 to 5 T, indicating that the oxide phases achieve magnetic saturation at considerably higher applied fields than in the corresponding coarse grained materials.

To study the magnetic behavior of both the oxides, the contribution of metallic iron was subtracted from the XMCD spectra. In this way, we provided evidence for a structural disorder-driven spin canting that predominantly affects Fe atoms that occupy octahedral sites. In particular, it was found that the amplitude of this magnetic disorder increases with increasing structural disorder and decreases upon the application of a stronger magnetic field. At the moment, the cause of this site specific spin canting is still subject of investigation.

From a methodological point of view, in this study we illustrate how XMCD may be used to study properties of magnetically complex systems. In particular, it is found to be a suitable tool to study even highly disordered and strained nanocrystalline solids and to distinguish magnetic contributions from different phases and crystallographically inequivalent sites.

ACKNOWLEDGMENTS

This work was partially supported by the European Union under the Improving Human Potential action (IHP) of the Fifth Framework Programme (FP5). The authors want to thank especially Massimiliano Marangolo of INSP for stimulating discussions and for providing, with N. Menguy of IMPMC, a preliminary characterization of investigated samples. We are also indebted to the skillful and technical support from the staff of the BACH beamline. Christophe Cartier dit Moulin is acknowledged for his help during the experiments.

¹P. Moriarty, Rep. Prog. Phys. **64**, 297 (2001).

²*Handbook of Nanostructured Materials and Nanotechnology*, Synthesis and Processing edited by H. S. Nalwa, Volume 1: (Academic, San Diego, 2001).

³R. C. O'Handley, *Modern Magnetic Materials: Principles and Application* (Wiley, New York, 2000).

⁴J. L. Dormann and D. Fiorani, *Magnetic Properties of Fine Particles* (Delta Series, North Holland, 1992).

⁵D. Weller, *7th International Conference on Nanostructured Mater (NANO2004)*, Wiesbaden, 2004, Vol. 4.

⁶N. Tsuda, K. Nasu, A. Fujimori, and K. Shiratori, *Electronic Conduction in Oxides*, 2nd ed. (Springer-Verlag, Berlin, 2000).

⁷C. G. Granqvist and R. A. Buhrman, J. Appl. Phys. **47**, 2200 (1976).

⁸K. Haneda and A. H. Morrish, Nature (London) **282**, 186 (1979).

⁹S. Gangopadhyay, G. C. Hadjipanayis, B. Dale, C. M. Sorensen, K. J. Klabunde, V. Papaefthymiou, and A. Kostikas, Phys. Rev. B **45**, 9778 (1992).

¹⁰L. Del Bianco, D. Fiorani, A. M. Testa, E. Bonetti, L. Savini, and S. Signoretti, Phys. Rev. B **66**, 174418 (2002).

¹¹L. Signorini, L. Pasquini, L. Savini, R. Carboni, F. Boscherini, E. Bonetti, A. Giglia, M. Pedio, N. Mahne, and S. Nannarone, Phys. Rev. B **68**, 195423 (2003).

¹²L. Theil Kuhn, A. Bojesen, L. Timmermann, M. Meedom Nielsen, and S. Mørup, J. Phys.: Condens. Matter **14**, 13551 (2002).

¹³E. Tronc, A. Ezzir, R. Cherkaoui, C. Chanéac, M. Noguès, H. Kachkachi, D. Fiorani, A. M. Testa, J. M. Grenèche, and J. P. Jolivet, J. Magn. Magn. Mater. **221**, 63 (2000).

¹⁴G. Schütz, W. Wagner, W. Wilhelm, P. Kienle, R. Zeller, R. Frahm, and G. Materlik, Phys. Rev. Lett. **58**, 737 (1987).

¹⁵C. T. Chen, F. Sette, Y. Ma, and S. Modesti, Phys. Rev. B **42**, R7262 (1990).

¹⁶C. T. Chen, Y. U. Idzerda, H.-J. Lin, G. Meigs, A. Chaiken, G. A. Prinz, and G. H. Ho, Phys. Rev. B **48**, R642 (1993).

¹⁷L. Savini, E. Bonetti, L. Del Bianco, L. Pasquini, L. Signorini, M. Coisson, and V. Selvaggini, J. Magn. Magn. Mater. **262**, 56 (2003).

¹⁸K. Fauth, E. Goering, G. Schutz, and L. Theil Kuh, J. Appl. Phys. **96**, 399 (2004).

¹⁹L. Del Bianco, D. Fiorani, A. M. Testa, E. Bonetti, and L. Signorini, Phys. Rev. B **70**, 052401 (2004).

²⁰L. Lutterotti and P. Scardi, J. Appl. Crystallogr. **23**, 246 (1990); *International Conference on Textures of Materials (ICOTOM-12)*, Montreal (1999), p. 1599.

²¹H. M. Rietveld, Acta Crystallogr. **20**, 508 (1966).

²²M. Zangrando, M. Finazzi, G. Paolucci, G. Comelli, B. Diviacco, R. Walker, D. Cocco, and F. Parmigiani, Rev. Sci. Instrum. **72**, 1313 (2001).

²³Ph. Saintavirt and J.-P. Kappler, *Magnetism and Synchrotron Radiation*, Vol. 256 of Lecture Notes in Physics (Springer-Verlag Berlin, 2001).

- ²⁴J. Stöhr and Y. Wu, *New Directions in Research with Third-Generation Soft X-Ray Synchrotron Radiation Sources*, Vol. 254 of NATO ASI Series (Kluwer Academic, Dordrecht, 1994).
- ²⁵F. de Groot, Chem. Rev. (Washington, D.C.) **101**, 1779 (2001); J. Electron Spectrosc. Relat. Phenom. **67**, 529 (1994).
- ²⁶Ch. Brouder and J.-P. Kappler, *Magnetism and Synchrotron Radiation*, Lecture Notes in Physics (Les Editions de Physiques, Les Ulis, 1997).
- ²⁷R. W. Siegel, *Mechanical Properties and Deformation Behavior of Materials Having a Ultra-Fine Microstructures*, Vol. 233 of NATO ASI Series (Kluwer Academic, Dordrecht, 1993).
- ²⁸R. Wu and A. J. Freeman, Phys. Rev. Lett. **73**, 1994 (1994).
- ²⁹P. Kuiper, B. G. Searle, L.-C. Duda, R. M. Wolf, and P. J. van der Zaag, J. Electron Spectrosc. Relat. Phenom. **86**, 107 (1997).
- ³⁰E. Pellegrin, M. Hagelstein, S. Doyle, H. O. Moser, J. Fuchs, D. Vollath, S. Shuppler, M. A. James, S. S. Saxena, L. Niesen, O. Rogojanu, G. A. Sawatzky, C. Ferrero, M. Borowsky, O. Tjernberg, and N. B. Brookes, Phys. Status Solidi B **215**, 797 (1999).
- ³¹P. Morrall, F. Schedin, G. S. Case, M. F. Thomas, E. Dudzik, G. van der Laan, and G. Thornton, Phys. Rev. B **67**, 214408 (2003).
- ³²S. Brice-Profeta, Ph.D thesis, Université "Pierre et marie Curie," Paris, 2004.
- ³³S. Brice-Profeta, M.-A. Arrio, E. Tronc, N. Menguy, I. Letard, C. Cartier dit Moulin, M. Noguès, C. Chanéac, J.-P. Jolivet, and Ph. Sainctavit, J. Magn. Magn. Mater. **288**, 354 (2005).
- ³⁴J. P. Wright, J. P. Attfield, and P. G. Radaelli, Phys. Rev. B **66**, 214422 (2002).
- ³⁵C. Greaves, J. Solid State Chem. **49**, 325 (1983).
- ³⁶R. M. Cornell and U. Schwertmann, *The Iron Oxides: Structure, Properties, Reactions, Occurrences and Uses* (Kiley VCH, Weinheim, 1994).
- ³⁷F. Sette, C. T. Chen, Y. Ma, S. Modesti, and N. V. Smith, *X-Ray Absorption Fine Structure* (Hellis Horwood, New York, 1991).
- ³⁸R. H. Kodama, J. Magn. Magn. Mater. **200**, 359 (1999).
- ³⁹J. Hunter Dunn, D. Arvanitis, N. Martensson, M. Tischer, F. May, M. Russo, and K. Baberschke, J. Phys.: Condens. Matter **7**, 1111 (1995).
- ⁴⁰R. Nakajima, J. Stöhr, and Y. U. Idzerda, Phys. Rev. B **59**, 6421 (1999).
- ⁴¹N. Guigue-Millot, Y. Champion, M. J. Hytch, F. Bernard, S. Bégin-Colin, and P. Perriat, J. Phys. Chem. B **105**, 7125 (2001).
- ⁴²E. Bonetti, L. Del Bianco, and S. Signoretti, J. Appl. Phys. **89**, 1806 (2001).